Heliyon

Received:
3 January 2019
Revised:
8 February 2019
Accepted:
20 March 2019

Cite as: Abdou Dia, Lamine Dieng, Laurent Gaillet, Papa Birame Gning. Damage detection of a hybrid composite laminate aluminum/glass under quasi-static and fatigue loadings by acoustic emission technique. Heliyon 5 (2019) e01414.
doi: 10.1016/j.heliyon.2019.e01414

Damage detection of a hybrid composite laminate aluminum/glass under quasi-static and fatigue loadings by acoustic emission technique

Abdou Dia [a], **Lamine Dieng** [a,*], **Laurent Gaillet** [a], **Papa Birame Gning** [b]

[a] *IFSTTAR, MAST, Bouguenais, France*

[b] *DRIVE–ISAT, Université de Bourgogne, 58027 Nevers, France*

[*] Corresponding author.

E-mail address: lamine.dieng@ifsttar.fr (L. Dieng).

Abstract

This paper deals with the characterization by Acoustic Emission technique of damages occurring in a hybrid laminate aluminium/glass during quasi-static and fatigue tests. Indeed, hybrid laminates materials metal/composites are more and more considered in structure, automotive and aerospace designs because of their good mechanical performances and lightness. To understand their damages characteristics, several types of laminates (fiber orientations, number of folds, presence or not of an aluminium sheet) have been tested. The acoustic emission analysis has been realized using statistical multi-parameters methods of data clustering: combination of Principal Components Analysis (PCA) and k-means methods in unsupervised analysis and Classification and Regression Trees (CART) in supervised analysis. Using these methods, it was possible to identify damages occurring during both quasi-static and fatigue tests. Acoustic emission parameters such as counts to peak (PCNTS), amplitude, duration, counts and frequency come out as the most relevant to classify the damage mechanisms; and with the energy parameter, friction mechanisms that can occur during fatigue tests have been sorted.

Keywords: Acoustics, Materials science, Mechanical engineering

https://doi.org/10.1016/j.heliyon.2019.e01414

1. Introduction

The use of the multi-component materials associating layers of metals and fibers reinforced polymer (FRP) composite folds, known as Fiber Metal Laminates (FML), is more and more expanding because of the increasing demand for aerospace and automotive applications and also in civil engineering [1]. Due to their hybrid aspect, FML materials combine advantages of both constituents, i.e. high mechanical and insulation properties of FRP layers and ductility with thermal and electrical conduction of the metal layers. Hence, several studies [2, 3, 4, 5, 6] have highlighted the benefits of their use, such as high resistance to crack propagation, impact loading and corrosion, that increases the fatigue endurance and durability of FML. Thus given their mechanical functions and their exposure to environmental conditions, understanding their long-term behavior is a major challenge for their use in structures. Different damage mechanisms, depending on the basic constituents, lay-ups, manufacturing processes and loadings, can occur in such composites and may not be detected by visual inspection, but can dramatically reduce the tensile strength of a component. Classically, four damage mechanisms are observed in FRP composites. The matrix cracking (MC) damage which is the fracture of the resin bonding the fibers together when the latter is mechanically loaded or under matrix shrinkage during polymerization; and in [7], Richardson et al. emphasize that shear cracking of the composite matrix have been observed to initiate the failure process in composites. The delamination/decohesion (DD) damage corresponds to the interface matrix/fibers fracture and separation of layers from each other. Fiber cracking (FC) damage, also known as fiber fracture, indicates the ultimate failure in well-designed laminates. These damage mechanisms have been described and studied in different studies [3, 4, 8, 9, 10]. For FML, additional debonding (D) can occur between the adjacent FRP and metal layers resulting from shear stress in the adhesive between the fibers and the metal layer [5]. Indeed local shear deformations occurring in the adhesive (matrix) reduce the crack bridging efficiency of the fibers, consequently the crack growth rate increases [11] which will lead to a final failure of the laminate.

Since these different kinds of damages are to some extent inevitable, many Non-Destructive Testing (NDT) methods are developed to assess the integrity and safety of composites materials. In [12] and [13], S. Gholizadeh and Jolly et al. respectively provide a review of the most common used NDT methods such as the visual testing, ultrasonic testing, thermography, shearography, Eddy current, acoustic emission, etc. The acoustic emission is an effective method for imperfection analysis since it is a high sensitive one and allows detection of many different damages types caused by loadings [12] or environmental effects [14, 15]. Thus, using AE, many authors show the possibility to detect and identify damage mechanisms in composite materials by analyzing a single parameter of the acoustic emission (AE) signal such as the

https://doi.org/10.1016/j.heliyon.2019.e01414

frequency or the amplitude of AE signals. Indeed Takeda et al. [16], through amplitude distributions, distinguish various fracture processes on high compliant, glass-matrix composite; Kim et al. [17] and Eaton et al. [18] respectively used amplitude distributions for carbon fiber reinforced polymer (CFRP) and peak frequency content of carbon fiber/epoxy composites to discriminate the different damage mechanisms involved. However for these composites, CFRP, and for more complex composites as the FML or simply laminates combining unidirectional lay-ups with different fiber orientations, this single parametric analysis turns out insufficient. Fatih et al. [19] show that high frequency distributions is not always a good mean to discriminate AE events; and Eckles et al. [20] conclude that, due to AE amplitude ranges overlapping, an efficient damages identification of CFRP in fatigue becomes tricky. Therefore, to overcome this issue, combination of different parameters appears as a good alternative and is used in this paper. Thus statistical methods are developed for data processing as the well-known supervised and unsupervised analyses methods. Such methods are used in several studies to identify composites damages [8, 21, 22]. In this paper, the Principal Components Analysis (PCA) and the k-means methods are used for unsupervised analysis to reduce the number of parameters and run the clustering; and as a supervised analysis method, the Classification and Regression Trees (CART) is adopted.

2. Material & methods

2.1. Material and experimental set up

First, $[0]_4$, $[90]_4$ and $[\pm45]_4$ unidirectional (UD) laminate samples have been collected from 4-layer 380 × 380 mm^2 composite plates named respectively P1, P2 and P3 and with an average thickness of 1 mm. These plates are made of type E glass fibers prepregs with an epoxy resin (HexPly® M34) having respectively a density (ρ_f and ρ_m) of 2560 and 1260 kg/m^3 [23]. The prepreg sheet is made of respectively 90 % and 10 % of wrap and weft fibers with a basis weight (m_{sf}) of 632 g/m^2. The black-colored (in order to increase its UV resistance) resin has a mass rate of 32 %. Those samples have been tested so that the acoustic signatures of UD will be known and better characterize the four fiber metal laminates (FML), $[0_4/Al]_s$, $[90_4/Al]_s$, $[(\pm45)_2/Al]_s$ et $[90/0/\pm45/Al]_s$ named respectively P4, P5, P6 and P7. The UD laminates are layered symmetrically to the 1 mm thick AG4MC (5086) aluminum sheet of 2650 kg/m^3 density. The aluminum sheet surface finishing has been done with a sandpaper to improve its adhesion with the prepreg.

The laminates have been stacked into a rigid steel mold and compressed at 3 bar in a compression-molding machine heated at 2 °C/min until 60 °C, followed by a constant temperature stage of 90 minutes, before final air cooling step. The thermo-compression process has been followed by post-curing stage at 90 °C during 90 minutes to ensure total reticulation of the matrix.

https://doi.org/10.1016/j.heliyon.2019.e01414

The volume fraction of fibers (V_f), aluminum (V_{alu}) and matrix (V_m) calculated by relations Eqs. (1) and (2) as in ASTM D3171-15 standard [24], density (ρ_c) (Eq. (3)) and mean thickness (t) of P1 to P7 are given in Table 1.

$$V_f = n \times m_{sf} / (\rho_f \times t) (n \ represents \ the \ number \ of \ plies) \quad (1)$$

$$V_{alu} = t_{alu}/t \quad (2)$$

$$\rho_c = V_f \rho_f + V_{alu} \rho_{alu} + V_m \rho_m \quad (3)$$

As recommended by Levesque [25], straight-sided specimens have been used. The latters are 250 mm long and 25 mm large and have been prepared from the fabricated plates. To avoid the grips of the testing machine to damage the specimens, they have been equipped with 1 mm (t_{alu}) thick aluminum end tabs (Fig. 1), accordingly to the ASTM D 3039 standard [26].

The specimens were equipped with strain gauge of 20 mm long and 2.12% maximum strain, adhesively bonded to their center. Two piezoelectric sensors (of type micro80 with operating frequency range of 175 kHz − 1 MHz and a resonant frequency of 350 kHz) were placed at 12.5 mm from each end tab in order to record the AE events and avoid parasitic noise which can be generated by the hydraulic grips of the testing machine. The AE signals have been recorded with CATMAN software and MISTRAS toolbox. The latter consists of a monitor to get the signals and proceed to the extraction of acoustic data in real time, the amplifier (c) and the preamplifier (d) of bandwidth from 32 to 1100 kHz (Fig. 2). A servo-hydraulic machine LOSEN SYSTEM with a capacity of 300 kN has been used to perform the quasi-static tests with a constant crosshead speed of 2 mm/min, and fatigue tests with a frequency of 3 Hz and a load level (F_{max}) of 60 % of the ultimate tensile strength (F_{UTS}) determined for each specimen according to previous tensile tests. Tensile−tensile fatigue tests have been conducted under load amplitude control and with a loading ratio of $R = \frac{F_{min}}{F_{max}} = 0.1$ to avoid the compression of specimens.

2.2. AE signal clustering methods

During a quasi-static or fatigue test, fifteen parameters of the AE's signals are recorded. However for an easier analysis and time saving, it was necessary to downsize

Table 1. Physical properties of hybrid laminates.

	V_f (%)	V_{alu} (%)	V_m (%)	ρ_c (g/cm^3)	t (mm)
P1−P3	51.5	-	48.5	1.93	1
P4−P7	40	30	30	2.20	3.32

https://doi.org/10.1016/j.heliyon.2019.e01414

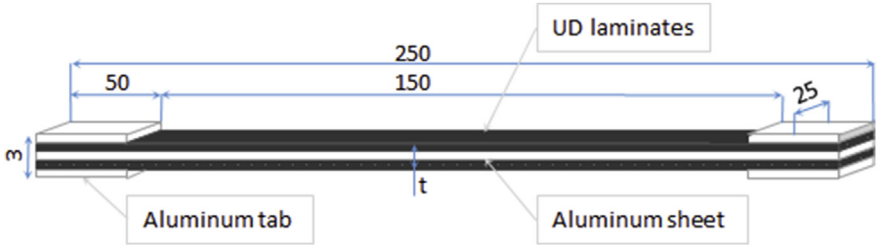

Fig. 1. Geometry of tensile laminates. Units are in mm.

the number of parameters. A set of AE parameters has been chosen according to their level of correlation [8] and the encompassed physical mechanisms.

To choose the minimal set of parameters, a Principal Components Analysis (PCA), through circles and matrices of correlation, allows determining the degree of correlation between parameters and their contribution on the ratio of information expressed by the k principal components. The k used parameters correspond to the k first axes (principal components) where the sum of the variances is superior or equal to 80 %. Thus, the following eight parameters have been used for the classification:

1. Rise Time (μs)
2. Counts
3. Energy (Arbitrary Units)
4. Amplitude (dB)
5. PCNTS (Counts to peak)
6. Signal strength (nVs)
7. Absolute energy (aJ)
8. Centroid frequency (kHz)

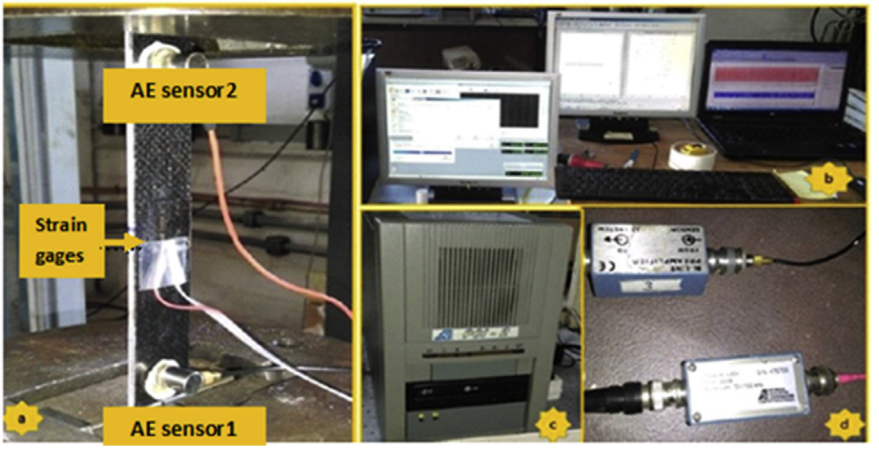

Fig. 2. Monitoring system: (a): AE sensors, (b): monitor, (c): amplifier and (d): preamplifier of bandwidth 32−1100 kHz.

https://doi.org/10.1016/j.heliyon.2019.e01414

With these parameters, we process to the identification of the AE signals by statistical multi-parametric analyses.

The method of k-means used in unsupervised analysis aims at minimizing the quadratic error for a given number of classes which have a Gaussian distribution around the center of each class. The algorithm is performed in six (6) steps (Fig. 3):

Two criteria have been fixed to initialize the algorithm by choosing an appropriate number of clusters (k). The first one is the Davies and Bouldin coefficient, R_{DB}, which gives information about the clusters compactness and is given by (Eq. (4)) [27]:

$$R_{DB} = \frac{1}{k}\sum_{i=1}^{k} \max_{i \neq j}\left(\frac{d_i + d_j}{D_{ij}}\right) \tag{4}$$

where k refers to number of clusters, d_i and d_j are the means within i and j clusters respectively and D_{ij} is the average distance between the clusters i and j. The best clustering is given by the lowest Davies and Bouldin coefficient.

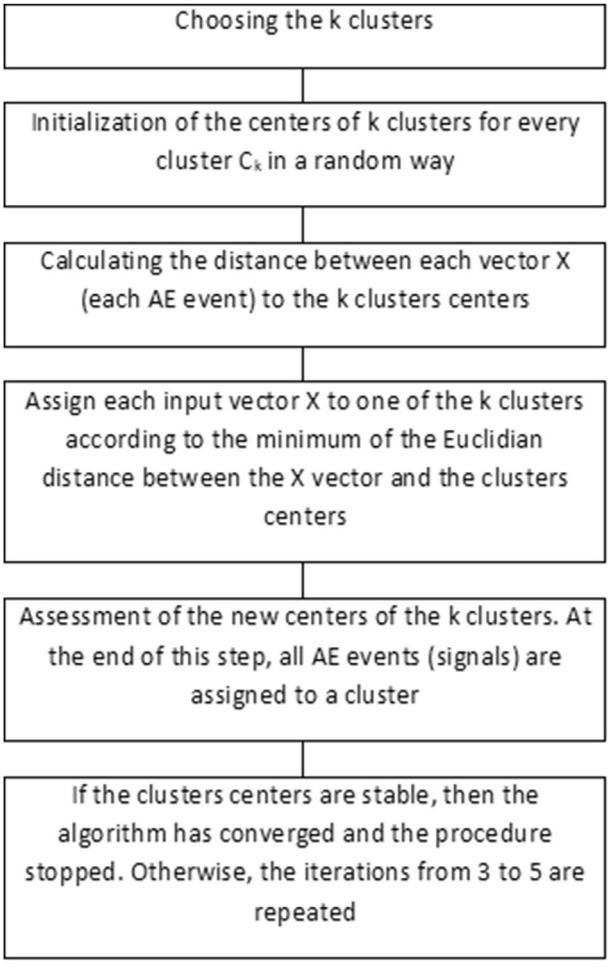

Fig. 3. Algorithm of the k-means method.

https://doi.org/10.1016/j.heliyon.2019.e01414

The second criterion is the physical coherence of the classification made on the data. For most of the analyzed data in this paper, the optimal number of predicted clusters by R_{DB} is coherent with the number of damage modes which can occur in a given laminate.

The Classification and Regression Trees (CART) method used in unsupervised analysis is an iterative method, based on a recursive partitioning methodology of the data. Indeed, the method builds clusters of individuals, the most homogeneous possible, by asking a succession of binary questions on the attributes of every individual [28].

3. Results & discussion

3.1. Quasi-static tests

The mean values of ultimate strengths measured from quasi-static tensile tests for all specimens, necessary before performing fatigue tests, are given in Table 2.

After quasi-static tests, the main fracture surfaces noticed are shown on Fig. 4. For $[0°]_4$ specimens (Fig. 4a), the main final cracks are longitudinal matrix cracks and fibers cracks. For $[90°]_4$ specimens (Fig. 4b), there is a brittle fracture orthogonal to the loading axis which is matrix crack. For $[\pm 45°]$ specimens (Fig. 4c), we have 45° oriented fractures. Hybrid laminates (Fig. 4d), in addition to debonding (D) between composite layers and the aluminum sheet, present similar modes of damages to those already quoted.

The damage modes depicted have been identified thanks to AE clustering using the free data mining software TANAGRA [29] with an excel plugin which allows importing directly experimental.

- **P1 $[0]_4$ and P4 $[0_4/Al/0_4]$**

For the $[0°]_4$ laminates (Fig. 5a), two clusters have been identified. The first one, named class1, includes 20% of the AE events and increases rapidly at the end of the test while the second one, named class2, with 80% of the AE, increase from the first moments of the test.

Compared to the cracks observed on these laminates specimens (Fig. 4a), the class2 could correspond to the longitudinal matrix cracks which are much more

Table 2. Quasi-static ultimate tensile strength of all specimens.

Laminates	Non hybrid laminates			Hybrid laminates			
	P1	P2	P3	P4	P5	P6	P7
F_{UTS} (kN)	25.40	2.13	4.06	54.99	9.64	14.71	20.78

https://doi.org/10.1016/j.heliyon.2019.e01414

Fig. 4. Specimens fracture surfaces: (a): P1, (b): P2, (c): P3, (d): P4; (e): P5, (f): P6, (g): P7.

numerous. Hence the class1 would correspond to fibers cracks which appear during the end of the test. Indeed in [30], the author identified a similar behavior of fibers cracks with Carbon Fiber Reinforced Polymers (CFRP). To confirm this classification, we also represent the amplitude vs centroid frequency (Fig. 6) of these classes.

From Fig. 6, the amplitudes of the class2, identified as matrix crack, rank from 35 to 45 dB and its frequencies from 280 to 320 kHz. The amplitudes of the class1, go up to 95 dB and its frequencies rank from 300 to 350 kHz; this is in agreement with the literature which identifies the fibers cracking as the minority damages appearing at tests ending with amplitudes higher than the other degradation mechanisms [31, 32, 33].

For the P4 ($[0_4/Al/0_4]$) specimens, besides the spurious data, three classes are identified (Fig. 5b). These so-called spurious data correspond to a very few number of AE events (0.3 %) with very high values compare to the others. In addition to the classes identified in P1 ($[0_4]$), the only class we can expect from the P4 specimens is the debonding (D) between composite layers and aluminum sheet. Almost all of the AE events associated with the class1 identified on Fig. 5b appear towards the

https://doi.org/10.1016/j.heliyon.2019.e01414

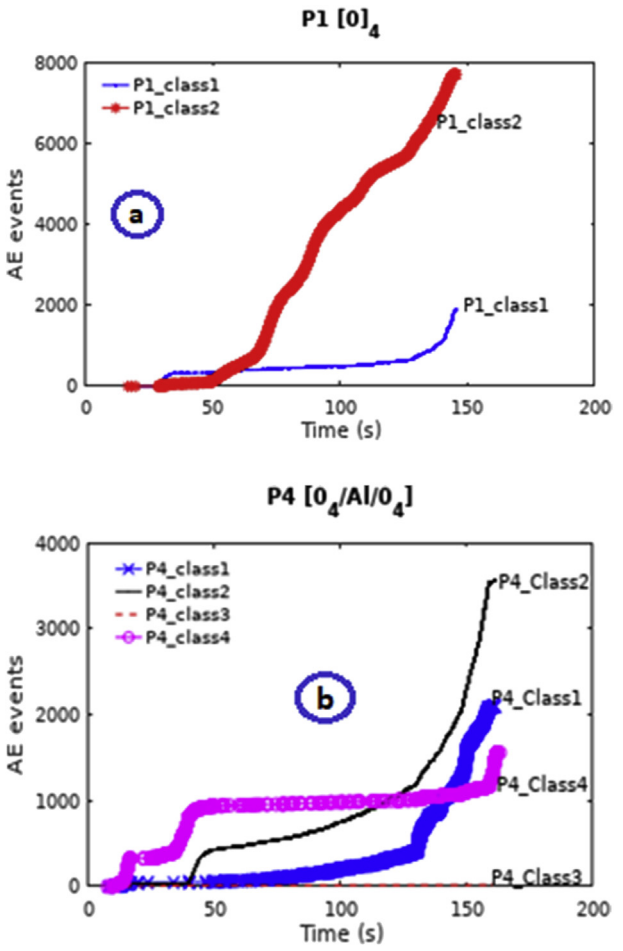

Fig. 5. (a) P1 and (b) P4 Clusters plotted in number of AE events vs time (s).

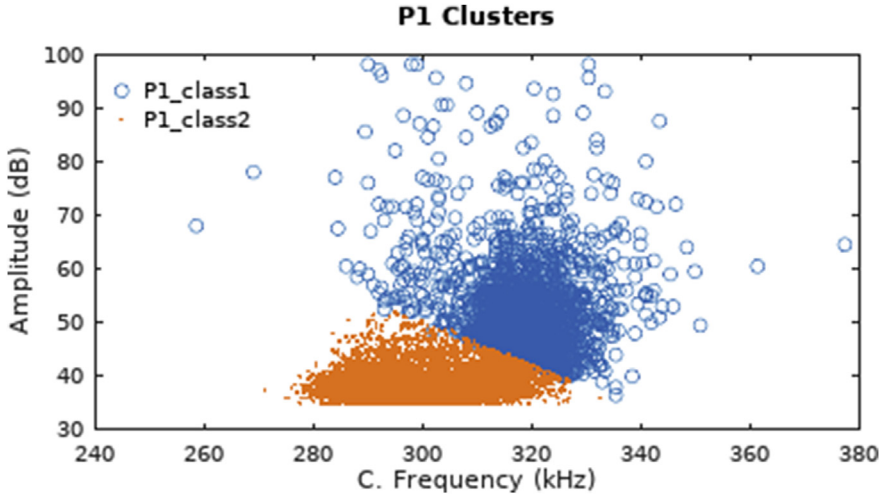

Fig. 6. P1 classes plotted in amplitude (dB) vs centroid frequency (kHz).

https://doi.org/10.1016/j.heliyon.2019.e01414

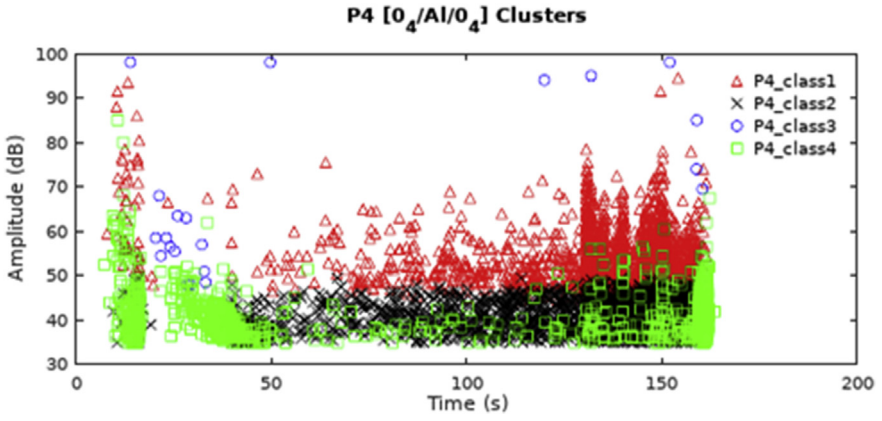

Fig. 7. P4 classes plotted in amplitude (dB) vs time (s).

end of the test with high amplitudes, as it can be seen on Fig. 7. Therefore, this class1 would correspond to the fractures of fibers.

To confirm this assumption, a supervised analysis of P1 data with P4 data has been performed. Therefore, the idea with the supervised analysis is to identify the two classes of P4 corresponding to the two classes identified with P1 specimens (MC and FC); and the non-identified one should be the debonding. Doing this, each event of P1 data will be classified in one of these three classes of P4.

Through the supervised analysis, instead of having all the events of P1 classified in only two classes (matrix cracking and fiber cracking) as in the unsupervised analysis, they are classified into three classes (class1, class2 and class4 of P4). This can be explained by the similarity between matrix cracking and debonding which are both polymers fractures. A comparison between the following figures (Fig. 8a and b) and Fig. 5a shows that the class1 of P4 corresponds to the class1 of P1 and thus to fiber cracking (FC). Furthermore, 54% and 34% respectively of the class4 and class2 of P4 are identified to the class2 of P1, i.e. as matrix cracking.

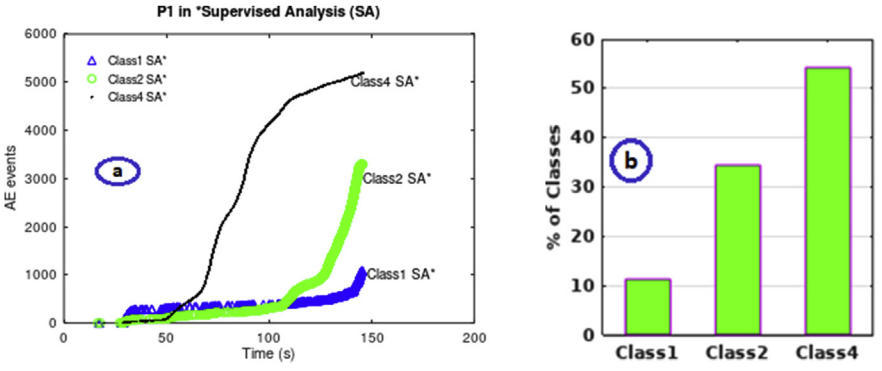

Fig. 8. (a): P1 clusters in unsupervised analysis plotted in AE events vs time (s), (b): clusters' percentages histogram.

https://doi.org/10.1016/j.heliyon.2019.e01414

Therefore, we can conclude that the class1 of P4 corresponds to the fiber cracking (FC), the class4 to the matrix cracking (MC), the class2 to debonding (D) and the class3 to spurious data.

- **P3 $[\pm 45]_2$ and P6 $[(\pm 45)_2/Al/(\pm 45)_2]$**

According to the Davies and Bouldin coefficient, three classes were determined for the P3 laminate as shown in Fig. 9. The three clusters correspond to the three classes which are matrix cracking (MC), delamination/decohesion (DD) and fiber cracking (FC). The time of occurrence of the mechanisms and their percentages show that the class1 corresponds to the fiber cracking and this class has the higher amplitudes and energy values (Fig. 10). A similar reasoning about the class2 and class3 allows us to classify them respectively as matrix cracking (MC) and delamination/decohesion (DD).

To perform the analysis of P6 laminates, after filtering the spurious data (0.1%) of the class3, four classes were identified (Fig. 11). class1 and class4 have similar curve evolution and represent respectively 34% and 31 % of the AE events. Except for the class5, the class4 has the highest amplitudes values and thus corresponds to the delamination/decohesion (DD); and class1, with the lowest values, to the matrix cracking (MC). Class5 corresponds to the fiber cracking (FC) since it has the highest amplitudes and the lowest AE events. The remaining class2 (25% of the AE events), with amplitude, PCNTS and counts values in the range of those of matrix cracking, corresponds to the debonding (D).

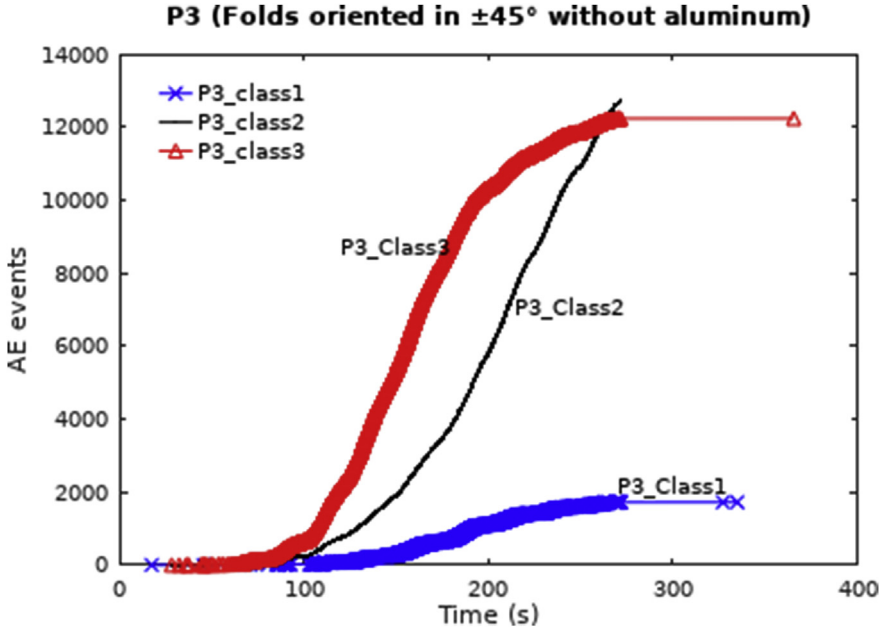

Fig. 9. P3 clusters in cumulative AE events vs time (s).

https://doi.org/10.1016/j.heliyon.2019.e01414

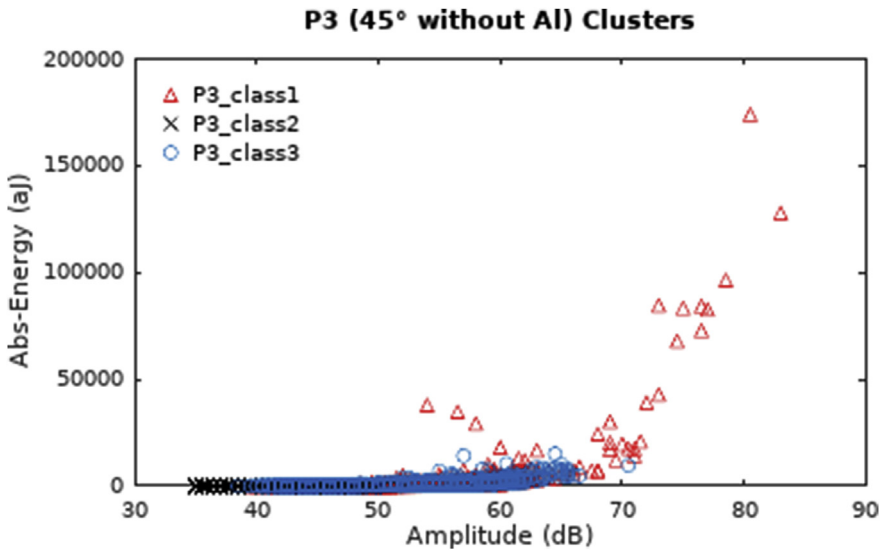

Fig. 10. P3 clusters plotted in absolute energy (aJ) vs amplitude (dB).

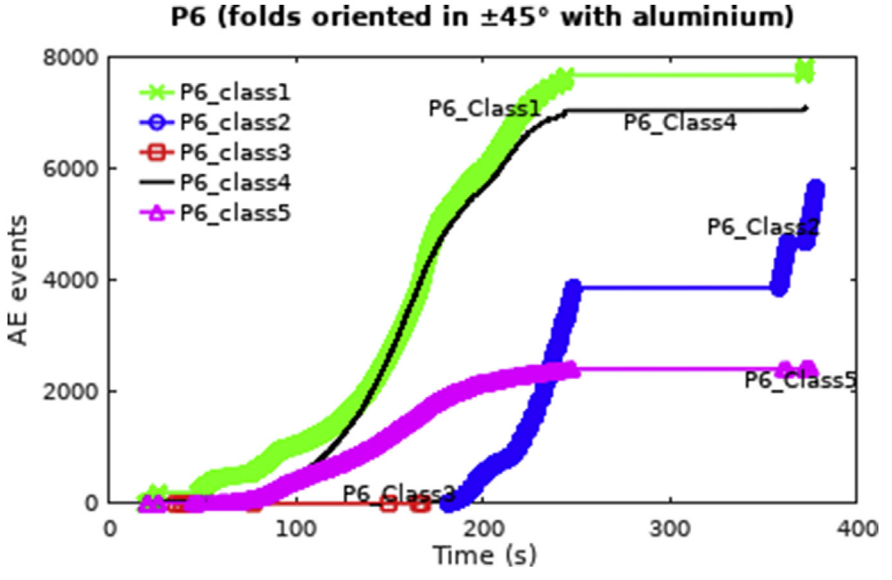

Fig. 11. P6 clusters in cumulative AE events vs time (s).

By averaging five AE parameters (counts, energy, duration, amplitude and PCNTS), a global histogram for P6 is built (Fig. 12) which confirms the previous classification. The calculated values are given in Table 3 in which the correlation between classes and damage mechanisms has been observed.

- **P2 $[90]_4$ and P5 $[90_4/Al/90_4]$**

Data of P2 laminates are not statistically analyzed since there is only a single damage mechanism, matrix cracking. However, this data is used to separate the two clusters of P5. This latter has two classes with similar values, matrix cracking and debonding

https://doi.org/10.1016/j.heliyon.2019.e01414

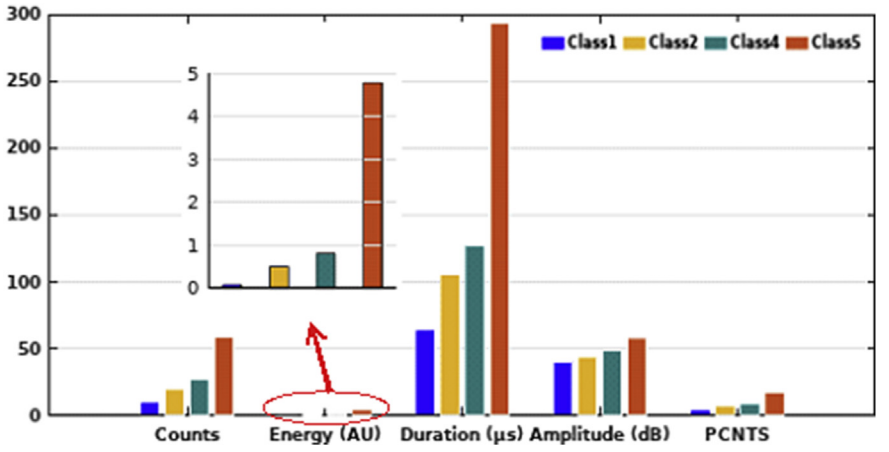

Fig. 12. P6 histogram based on the mean values of counts, energy, duration, amplitude and PCNTS.

Table 3. Correlation between P6 classes and damage mechanisms with mean values of five parameters.

Classes	Counts	Energy (AU)	Duration (µs)	Amplitude (dB)	PCNTS	Damages
Class1	10.07	0.08	63.86	40.41	4.34	Matrix cracking (MC)
Class2	19.43	0.50	105.67	43.45	6.88	Debonding (D)
Class4	26.74	0.81	127.36	48.29	8.87	Delamination/decohesion (DD)
Class5	58.30	4.79	293.50	57.74	17.08	Fibers cracking (FC)

(D). Matrix cracking of P5 is identified by comparing its values with those of P2 (which includes only this mechanism). The mean values of the five parameters used above are reported in a histogram (Fig. 13).

Table 4 highlights the relationship between classes and damage mechanisms from the mean values of the AE parameters.

- **P7 [90/0/+45/-45/Al/-45/+45/0/90]**

Clustering is done with five classes (Fig. 14) where the class3 corresponds to the spurious data.

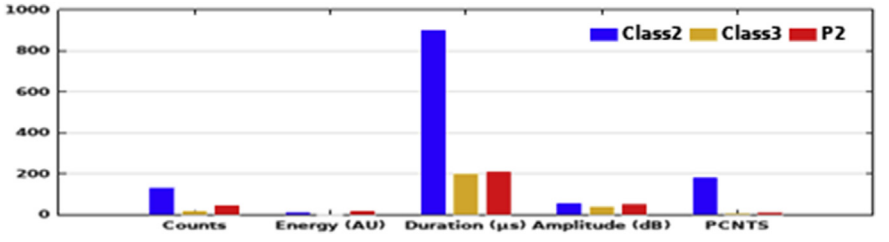

Fig. 13. P5 histogram based on the mean values of counts, energy, duration, amplitude and PCNTS compared to P2 values.

https://doi.org/10.1016/j.heliyon.2019.e01414

Table 4. Correlation between P5 classes and damage mechanisms with mean values of five parameters.

Classes	Counts	Energy (AU)	Duration (μs)	Amplitude (dB)	PCNTS	Damages
Class2	132.33	12.49	904.18	57.60	182.59	Debonding (D)
Class3	19.47	0.79	202.79	40.66	7.33	Matrix cracking (MC)

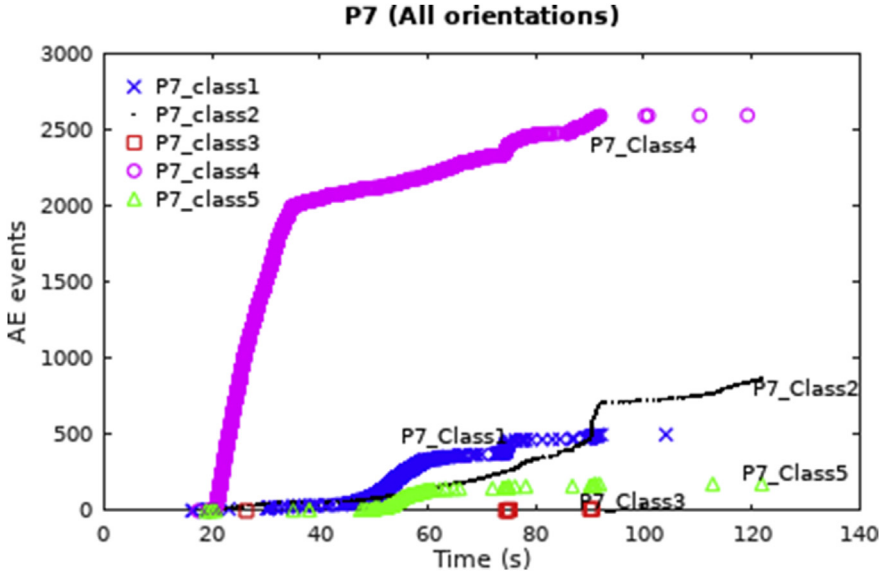

Fig. 14. P7 classes plotted in cumulative AE events vs time (s).

From Fig. 14, the only class that is very distinctive from the others is the class4 which represent 62% of the AE events. It appears from the beginning of the test and increases rapidly. Comparing its low amplitude and energy with the others on Fig. 15, we can assume class4 corresponds to matrix cracking.

On Fig. 15, the class5 has the highest values in amplitude and energy representing barely 4% of the AE events. These features can be related to fiber cracking (FC). The remaining classes, class1 and class2, correspond to debonding and delamination/decohesion (DD) and will be classified by comparing their values through the histogram of mean values (Fig. 16).

On that basis, the correlation between damage mechanisms and classes is established in Table 5.

3.2. Fatigue tests

The specimens tested in fatigue present similar **final fracture modes** to those tested in quasi-static tests (see Fig. 4).

https://doi.org/10.1016/j.heliyon.2019.e01414

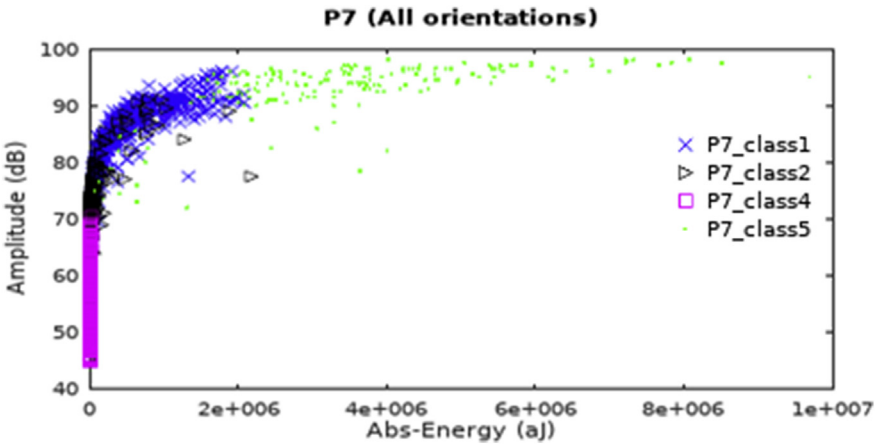

Fig. 15. P7 clusters in amplitude (dB) vs absolute energy (aJ).

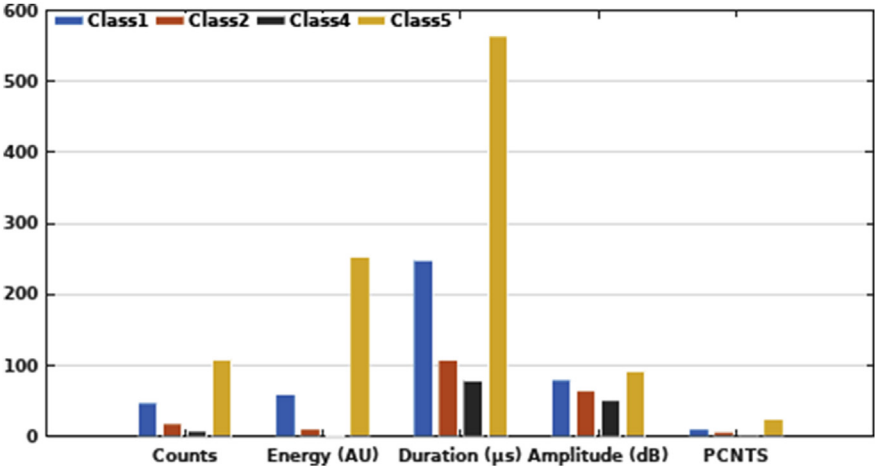

Fig. 16. P7 histogram based on the mean values of counts, energy, duration, amplitude and PCNTS.

During fatigue tests a large number of AE events were recorded. To avoid saturation of AE system, the threshold of 35 dB fixed during quasi-static and the first fatigue tests has been increased to 45 dB. This increase in AE events is due to the friction between opened cracks lips; this friction having low amplitudes and high frequencies [8].

Table 5. Correlation between P7 classes and damage mechanisms with mean values of five parameters.

Classes	Counts	Energy (AU)	Duration (µs)	Amplitude (dB)	PCNTS	Damages
Class1	47.52	59.77	248.39	79.84	10.48	Delamination/decohesion
Class2	18.18	10.61	108.05	64.47	6.34	Debonding
Class4	7.54	1.27	79.29	50.93	3.51	Matrix cracking
Class5	109.02	253.02	563.66	92.92	24.33	Fibers cracking

https://doi.org/10.1016/j.heliyon.2019.e01414

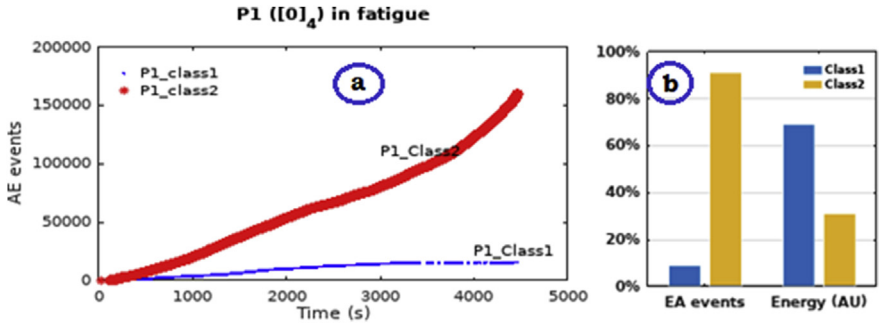

Fig. 17. (a): P1 clusters plotted in cumulative AE events vs time (s) with (b): histogram of energy and percentage of AE events.

In this second part of results, the same parameters and algorithms have been used for the statistical analysis and data clustering is made with the unsupervised analysis method.

- **P1 $[0]_4$ in fatigue**

According to the Davies and Bouldin coefficient, two clusters have been identified for this laminate. The class1, with 9% of the AE events, has the highest amplitudes and energy (Figs. 17 and 18). It, thus, corresponds to fiber cracking. This low percentage compared to the one obtained in quasi-static test is due to a higher number of events recorded that can be attributed to friction. Events that may be classified as matrix cracking include events of these friction mechanisms, grouped in the same class, matrix cracking (class2).

To discriminate these two mechanisms (matrix cracking and friction), the events belonging to the class2 were processed and classified into two others classes,

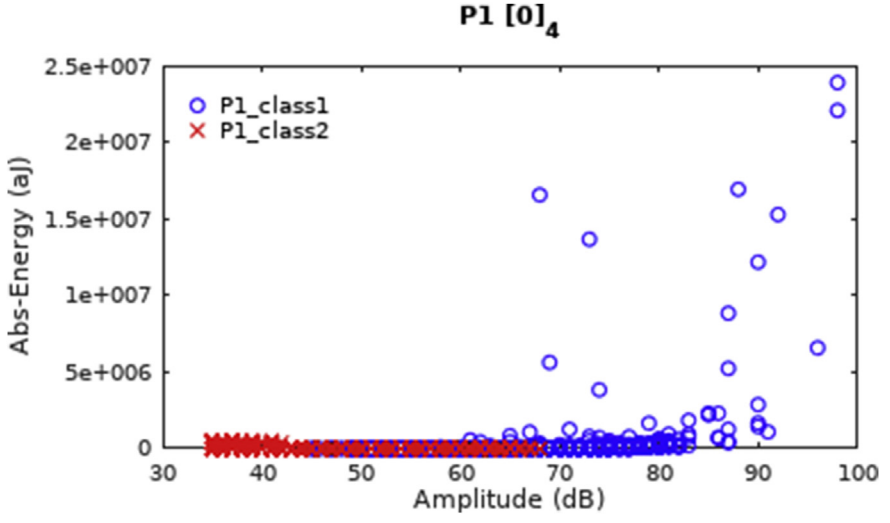

Fig. 18. P1 clusters in fatigue plotted in absolute energy (aJ) vs amplitude (dB).

https://doi.org/10.1016/j.heliyon.2019.e01414

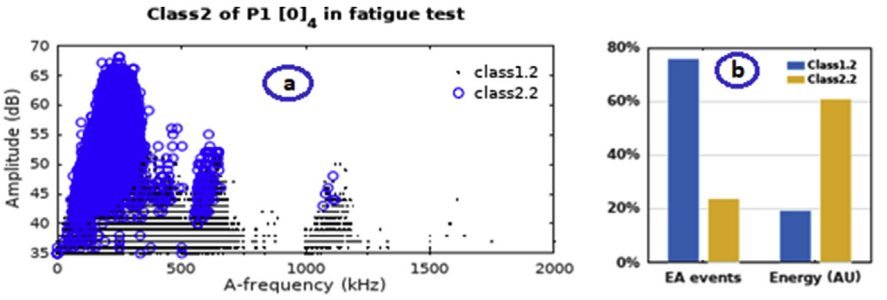

Fig. 19. (a): Classification of the class2 of P1 in average frequency (kHz) vs amplitude (dB) (b): Histogram of energy (AU) and AE events percentages of the class2 of P1.

class1.2 and class2.2. This classification has been based on amplitude and average frequency parameters. On Fig. 19a, it appears that the class1.2 has high frequencies and low amplitudes [35−45 dB]. Thus, according to the studies of R'Mili and al. mentioned above [8], the class1.2 is attributed to friction, and consequently the class2.2 to matrix cracking. It should be noticed that these friction mechanisms represent 76 % of the events of the class2 of P1 that is 60 % of all the recorded AE events. However, their energy remains very weak; indeed, it represents only 24 % of the energy of the class2 that is hardly 7 % of the total energy, Fig. 19b.

- **P3 $[\pm 45]_2$ in fatigue**

In this case, the Davies and Bouldin coefficient indicates three optimal clusters as in quasi-static results. To include the friction mechanisms, the clustering is done with four (4) clusters.

A histogram is elaborated considering the mean values of amplitude, energy, counts, counts to peak (PCNTS) and duration (Fig. 20). The class4 has the maximum values followed by the values of class2. Compared to the previous results, we can conclude that class4 corresponds to the fiber cracking (FC) and class2 to delamination/decohesion (DD).

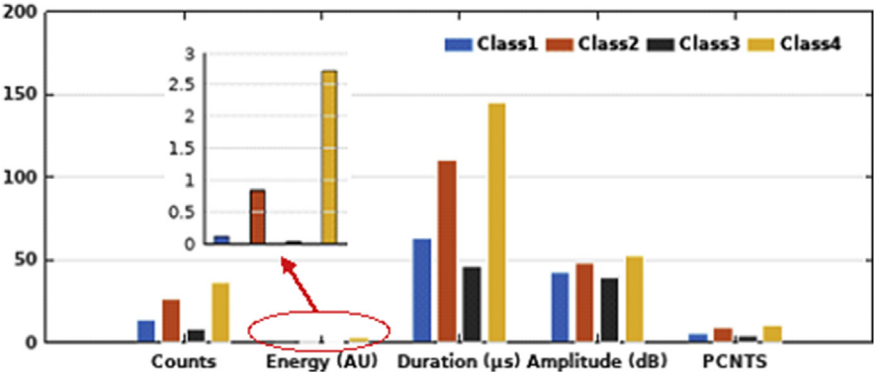

Fig. 20. P3 histogram based on the mean values of counts, energy, duration, amplitude and PCNTS.

https://doi.org/10.1016/j.heliyon.2019.e01414

To sort class1 and class3 in matrix cracking and friction mechanisms, one can notice that the class1's amplitudes are higher than those of the class3 but its frequencies are also the highest; this does not allow us to differentiate the two phenomena since we noticed that the mechanism, among these two, with the highest amplitudes had the lowest frequencies. However, we have previously noticed that the friction energy is very weak (60% of AE events for barely 7% of energy). Thus, by representing the histogram of energy of the classes (Fig. 21), it appears that the class3 (28% of the AE events for 1 % of the total energy) corresponds to the friction and the class1 (5% of the energy) to the matrix cracking. Fig. 21 confirms at the same time the classification made with the class4 and class2, i.e. they correspond respectively to FC and DD.

From all these analyses, one has observed that friction mechanism has low amplitudes [35−45 dB]. Thus, for the hybrid specimens (with an aluminum sheet) tested in fatigue where the threshold is fixed equal at least at 45 dB, this mechanism will not be taken into account. For the following analysis only the classification of P7 [90/0/+45/-45/Al/-45/+45/0/90] will be presented.

- **P7 in fatigue**

The four identified clusters are represented in Fig. 22.

To discriminate them, they are represented through the AE parameters previously selected using a histogram representation, Fig. 23.

According to Fig. 22, the following classification can be proposed:

- The class3, with the highest values, corresponds to fiber cracking (FC),
- The class1, having the highest values after those of FC to delamination/decohesion
- The class4, with the lowest values of classes 1/3/4 to debonding (D),

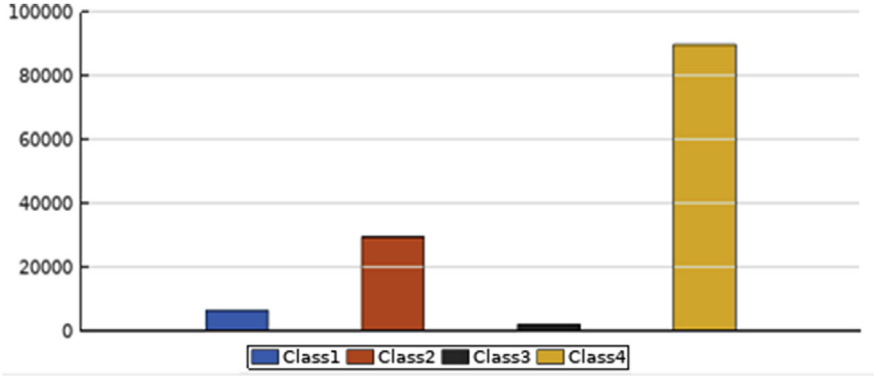

Fig. 21. Cumulative energy for P3 classes.

https://doi.org/10.1016/j.heliyon.2019.e01414

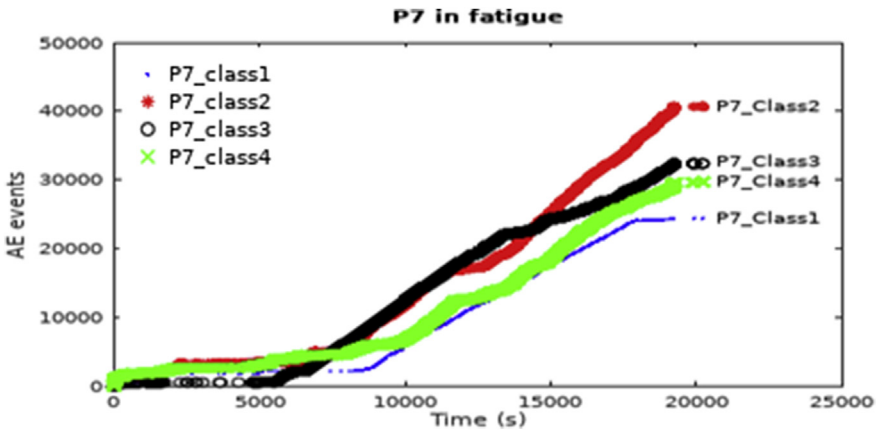

Fig. 22. P7 fatigue clusters plotted in cumulative AE events vs time (s).

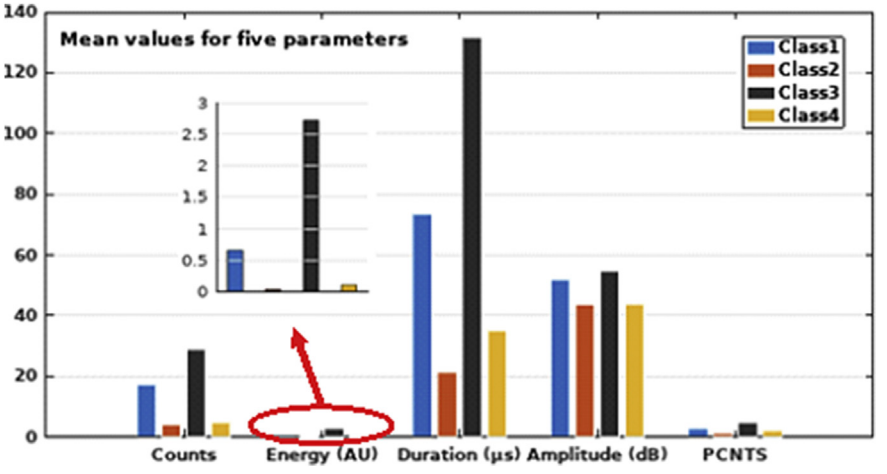

Fig. 23. P7 histogram in fatigue based on the mean values of counts, energy, duration, amplitude and PCNTS.

– The class2 with the highest number of AE events and the lowest values for these five parameters to the matrix cracking (MC).

4. Conclusion

In order to understand the long-term behavior of hybrid laminates, the damages occurring in FMLs have been monitored by acoustic emission (AE) method during quasi-static and fatigue tests. Using machine-learning tools and through an original approach based on the principle of breaking down a complicated problem into different more affordable pieces, the issue of identification and classification of multiple damages (MC, FC, D, DD, friction) occurring in the FML: [90/0/+45/-45/Al/-45/+45/0/90] during cycling loadings has been addressed. Therefore:

https://doi.org/10.1016/j.heliyon.2019.e01414

- With unsupervised analysis, k-means and PCA, it was possible to classify different similar damage mechanisms on the basis of a set of five AE parameters, namely matrix cracking and friction, matrix cracking and debonding or debonding and delamination/decohesion.
- Similarity between matrix cracking and debonding has been noticed (see supervised analysis of P1 with P4) with the CART method that comes out, by itself, insufficient to distinguish them until it is not combined with the results from unsupervised analysis.
- This statistical method (unsupervised analysis) allowed isolating the friction mechanisms that are very numerous in fatigue loads (about 60% of all the acoustic emission events) but with low energy.
- The different damage mechanisms occurring in tested laminates can be graded from their AE mean values.

It should then be interesting, using the two sensors, to locate the damage in order to improve the damage characterization and know which part of the material is more susceptible to initiate the damage.

To come over the issue of the system saturation during fatigue tests, an interesting option must be to use a continuous recording of AE waveforms as proposed in [34].

Declarations

Author contribution statement

Abdou Dia: Conceived and designed the experiments; Performed the experiments; Analyzed and interpreted the data; Contributed reagents, materials, analysis tools or data; Wrote the paper.

Lamine Dieng: Conceived and designed the experiments; Analyzed and interpreted the data; Contributed reagents, materials, analysis tools or data.

Papa Birame Gning: Conceived and designed the experiments; Contributed reagents, materials, analysis tools or data.

Laurent Gaillet: Analyzed and interpreted the data; Contributed reagents, materials, analysis tools or data.

Funding statement

This research did not receive any specific grant from funding agencies in the public, commercial, or not-for-profit sectors.

https://doi.org/10.1016/j.heliyon.2019.e01414

Competing interest statement

The authors declare no conflict of interest.

Additional information

No additional information is available for this paper.

Acknowledgements

Authors are thankful to the laboratory technicians Jean F. David and Yannick Falaise for their contribution to tests performing and results analysis.

References

[1] H. Nguyen, W. Zatar, H. Mutsuyoshi, Hybrid polymer composites for structural applications, in: Hybrid Polymer Composite Materials, Elsevier, 2017, pp. 35−51.

[2] L. Vogelesang, A. Vlot, Development of fibre metal laminates for advanced aerospace structures, J. Mater. Process. Technol. 103 (1) (Jun. 2000) 1−5.

[3] W. Roundi, A. El Mahi, A. El Gharad, J.-L. Rebiere, Acoustic emission monitoring of damage progression in glass/epoxy composites during static and fatigue tensile tests, Appl. Acoust. 132 (Mar. 2018) 124−134.

[4] B. Harris, Engineering Composite Materials, second ed., The Cambridge University Press, Cambridge, 1999.

[5] A. Vlot, J.W. Gunnink (Eds.), Fibre Metal Laminates an Introduction, Springer, Dordrecht, 2001.

[6] T. Pärnänen, M. Kanerva, E. Sarlin, O. Saarela, Debonding and impact damage in stainless steel fibre metal laminates prior to metal fracture, Compos. Struct. 119 (Jan. 2015) 777−786.

[7] M.O.W. Richardson, M.J. Wisheart, Review of low-velocity impact properties of composite materials, Compos. Part A Appl. Sci. Manuf. 27 (12) (Jan. 1996) 1123−1131.

[8] S. Momon, N. Godin, P. Reynaud, M. R'Mili, G. Fantozzi, Unsupervised and supervised classification of AE data collected during fatigue test on CMC at high temperature, Compos. Part A Appl. Sci. Manuf. 43 (2) (Feb. 2012) 254−260.

[9] M. Knops, Analysis of Failure in Fiber Polymer Laminates: the Theory of Alfred Puck, Springer, Berlin, 2008.

https://doi.org/10.1016/j.heliyon.2019.e01414

[10] E. Totry, J.M. Molina-Aldareguía, C. González, J. LLorca, Effect of fiber, matrix and interface properties on the in-plane shear deformation of carbon-fiber reinforced composites, Compos. Sci. Technol. 70 (6) (Jun. 2010) 970–980.

[11] R. Marissen, Fatigue Crack Growth in Arall a Hybrid Aluminium-Aramid Composite Material, Delft University of Technology, 1988.

[12] S. Gholizadeh, A review of non-destructive testing methods of composite materials, Proc. Struct. Integr. 1 (2016) 50–57.

[13] M. Jolly, et al., Review of non-destructive testing (NDT) techniques and their applicability to thick walled composites, Proc. CIRP 38 (Jan. 2015) 129–136.

[14] L. Michalcová, M. Kadlec, Carbon/epoxy composite delamination analysis by acoustic emission method under various environmental conditions, Eng. Fail. Anal. 69 (2016) 88–96.

[15] M. Perrin, L. Gaillet, C. Tessier, H. Idrissi, Hydrogen embrittlement of prestressing cables, Corros. Sci. 52 (6) (Jun. 2010) 1915–1926.

[16] N. Takeda, O. Chen, T. Kishi, W. Tredway, K. Prewo, Acoustic emission characterization of the fracture mechanism of a high compliant, glass-matrix composite, Eng. Fract. Mech. 40 (4) (1991) 791–799.

[17] S.-T. Kim, Y.-T. Lee, Characteristics of damage and fracture process of carbon fiber reinforced plastic under loading-unloading test by using AE method, Mater. Sci. Eng. A 234–236 (1997) 322–326.

[18] M. Eaton, K. Holford, C. Featherston, R. Pullin, Damage in carbon fibre composites: the discrimination of acoustic emission signals using frequency, J. Acoust. Emiss. 25 (2007).

[19] F.E. Oz, N. Ersoy, S.V. Lomov, Do high frequency acoustic emission events always represent fibre failure in CFRP laminates? Compos. Part A Appl. Sci. Manuf. 103 (Dec. 2017) 230–235.

[20] W. Eckles, J. Awerbuch, Monitoring acoustic emission in cross-ply graphite/epoxy laminates during fatigue loading, J. Reinf. Plast. Compos. 7 (3) (May 1988) 265–283.

[21] Y. Ech-Choudany, M. Assarar, D. Scida, F. Morain-Nicolier, B. Bellach, Unsupervised clustering for building a learning database of acoustic emission signals to identify damage mechanisms in unidirectional laminates, Appl. Acoust. (2017).

https://doi.org/10.1016/j.heliyon.2019.e01414

[22] M. Nazmdar Shahri, J. Yousefi, M. Fotouhi, M. Ahmadi Najafabadi, Damage Evaluation of Composite Materials Using Acoustic Emission Features and Hilbert Transform, 50, 2015.

[23] Hexcel Corporation, "HexPly_M34." [Online]. Available: http://www.hexcel.com/user_area/content_media/raw/HexPly_M34_eu_DataSheet.pdf. [Accessed 27 February 2018].

[24] ASTM D3171-15, Standard Test Methods for Constituent Content of Composite Materials, ASTM International, West Conshohocken, PA, 2015 [Online]. Available: https://www.astm.org.

[25] M. Levesque, L'essai de traction de matériaux composites unidirectionnels à fibres continues, Ecole Polytechnique de Montréal, Montréal, 2000.

[26] ASTM D3039/D3039M-17, Standard Test Method for Tensile Properties of Polymer Matrix Composite Materials, ASTM International, West Conshohocken, PA, 2017 [Online]. Available: https://www.astm.org.

[27] D.L. Davies, D. Bouldin, A cluster separation measure, PAMI 1 (1979).

[28] L. Breiman, Random forests, Mach. Learn. 45 (1) (2001) 5−32.

[29] R. Rakotomalala, TANAGRA : une plate-formed expérimentation pour la fouille de données, Rev. Modul. (2005) 70−85.

[30] C. Barile, Innovative mechanical characterization of CFRP by using acoustic emission technique, Eng. Fract. Mech. (Mar. 2018).

[31] S. Barré, M.L. Benzeggagh, On the use of acoustic emission to investigate damage mechanisms in glass-fibre-reinforced polypropylene, Compos. Sci. Technol. 52 (3) (1994) 369−376.

[32] T. Le Gall, Simulation de l emission acoustique: Aidè a l'identification de la signature acoustique des mécanismes d'endommagement, INSA, Lyon, 2016.

[33] A.A. Anastassopoulos, T.P. Philippidis, Clustering methodology for the evaluation of acoustic emission from composites, J. Acoust. Emiss. 13 (1−2) (1995) 11−22.

[34] K. Ito, M. Enoki, Acquisition and analysis of continuous acoustic emission waveform for classification of damage sources in ceramic fiber mat, Mater. Trans. 48 (6) (2007) 1221−1226.

https://doi.org/10.1016/j.heliyon.2019.e01414